https://doi.org/10.5194/egusphere-2026-3461
Preprint. Discussion started: 8 July 2026

Climatic controls on interannual mass balance of Arctic glaciers and ice caps

Xiaojun Ma[1], Matt A. King[2,3], Jonathan L. Bamber[4,5], Bin Liu[6], Wenke Sun[1], Qiuyu Wang[1,4]

[1]State Key Laboratory of Earth System Numerical Modeling and Application, College of Earth and Planetary Sciences, University of Chinese Academy of Sciences, Beijing, 100049, China
[2]School of Geography, Planning, and Spatial Sciences and Institute for Marine and Antarctic Studies, University of Tasmania, Hobart, TAS, 7001, Australia
[3]The Australian Centre for Excellence in Antarctic Science, University of Tasmania, Hobart, TAS, 7001, Australia
[4]Bristol Glaciology Centre, School of Geographical Sciences, University of Bristol, BS8 1SS, UK
[5]Chair of Data Science in Earth Observation, Department of Aerospace and Geodesy, Technical University of Munich, Munich, 80333, Germany
[6]School of Aeronautic Engineering, Changsha University of Science and Technology, Changsha, 410114, China

Correspondence to: Qiuyu Wang (wangqiuyu@ucas.ac.cn)

Abstract. Interannual variability in glacier and ice cap (GIC) mass balance can be large amplitude, masking the underlying decadal trends associated with external forcing. Here we apply Independent Component Analysis (ICA) to global GIC mass anomalies derived from the Gravity Recovery and Climate Experiment (GRACE) mission and GRACE Follow-On (GRACE-FO) satellite gravimetry missions over 2002–2024. We show that Arctic glacier regions dominate the leading interannual variability in the global gravimetry record, and account for more than two-thirds of recent global GIC mass loss. Two leading Arctic ICA modes explain ~75% of interannual variance and are associated with North Atlantic Oscillation (NAO)- and Pacific Decadal Oscillation (PDO)-related multi-year climate variability. Multiple linear regression further shows that variability linked to these climate modes explains much of the interannual glacier-mass variability in Arctic glacier regions and significantly affects trend estimates. This effect is most pronounced in Alaska, where the uncorrected trend is about 25% less negative than the value after accounting for this variability (-69 ± 21 Gt yr^{-1} versus -92 ± 16 Gt yr^{-1}). These results suggest that persistent North Atlantic and Pacific circulation variability can substantially change regional glacier mass loss, with direct implications for interpreting recent Arctic glacier change and their secular trends driven by external forcing.

1 Introduction

Glaciers and ice caps respond rapidly to climate forcing and variability, making their mass balance a sensitive indicator of both long-term warming (Rounce et al., 2023) and shorter-term climate fluctuations (Bolch et al., 2013; Hugonnet et al., 2021; Dussaillant et al., 2025; Marzeion et al., 2018; Bjørk et al., 2018). While the long-term global retreat of glaciers is well established (Zemp et al., 2025; Rounce et al., 2023; Hock et al., 2019; Otosaka et al., 2023; Jakob and Gourmelen, 2023; Hugonnet et al., 2021; Ciracì et al., 2020; Tapley et al., 2019; Zemp et al., 2019; Dussaillant et al., 2025; Tepes et al., 2021;

https://doi.org/10.5194/egusphere-2026-3461
Preprint. Discussion started: 8 July 2026

Wouters et al., 2019), precise records of regional mass change only exist through GRACE and GRACE-FO satellite gravimetry available only since 2002 (Jacob et al., 2012; Tapley et al., 2019; Ciracì et al., 2020; Sutterley et al., 2020; Bamber et al., 2018; Harig and Simons, 2016; Sasgen et al., 2024; Wang et al., 2021). The influence of multi-year climate variability on gravimetric estimates of glacier change is not yet clear (Tapley et al., 2019; Wouters et al., 2013; Bamber et al., 2018).

Multi-year climate variability can influence trend estimates derived from gravimetry records, biasing estimated mass-loss rates from their longer-term rates and introducing spurious regional differences and inter-study confusion (Jacob et al., 2012; King et al., 2012; Bamber et al., 2018; Tapley et al., 2019; Wouters et al., 2013; Harig and Simons, 2016; Tedesco et al., 2013; Wouters et al., 2019; Ciracì et al., 2020; Noël et al., 2022). Quantifying and mitigating this effect is clearly important (Bamber et al., 2018; Harig and Simons, 2016; Wouters et al., 2019; Wouters et al., 2013; King et al., 2012). This issue is especially relevant in Arctic glacier regions, which account for about two-thirds of recent global glacier mass loss (Jakob and Gourmelen, 2023; Hugonnet et al., 2021; Ciracì et al., 2020; Box et al., 2018; Zemp et al., 2019; Tepes et al., 2021; Wouters et al., 2019; Zemp et al., 2025) and exhibit pronounced interannual variability in GRACE/GRACE-FO observations, motivating a closer examination of the Arctic contribution to the global record.

For Arctic glaciers, the influence of Atlantic-sector climate variability has been more extensively documented than that of Pacific-sector variability. Both sectors provide pathways through which large-scale climate variability can be expressed in Arctic GIC mass change (Sasgen et al., 2024; Wouters et al., 2019). NAO-related North Atlantic circulation modulates temperature, precipitation and moisture transport across the Atlantic sector of the Arctic (Sasgen et al., 2024; Sasgen et al., 2022; Moon et al., 2018), and has been linked to surface-mass-balance (SMB) variability in the Canadian Arctic (Noël et al., 2018), Svalbard (Bonan et al., 2019; Lang et al., 2015) and the Russian Arctic (Maure et al., 2023). Pacific-sector variability, including the PDO, has been linked most directly to glacier mass-balance variability in Alaska (Arendt et al., 2009; Jakob et al., 2021), the largest source of recent mass loss among Arctic GIC regions (Zemp et al., 2025; Dussaillant et al., 2025; Jakob and Gourmelen, 2023; Ciracì et al., 2020). Year-to-year mass anomalies in most Arctic glacier regions arise primarily from SMB variability (Jakob and Gourmelen, 2023; Ciracì et al., 2020; Tepes et al., 2021), although marine-terminating sectors in the Barents and Kara Sea region can include an important dynamic component (Tepes et al., 2021; Ciracì et al., 2018; Li et al., 2025; Jakob and Gourmelen, 2023). These NAO- and PDO-related SMB signals should therefore be evident in Arctic GIC mass-change time series. Arctic-wide SMB reconstructions (Maure et al., 2023) further show that climate forcing produces spatially heterogeneous responses across the Arctic, suggesting that NAO- and PDO-related variability may be expressed in GRACE/GRACE-FO records as regionally contrasting mass-change patterns rather than as a spatially uniform signal.

Because GRACE/GRACE-FO observe cumulative mass change rather than mass flux, recent Antarctic studies have compared gravimetric mass-change records with cumulative forms of the climate indices that reflect the variability of various climate modes (Kim et al., 2020; Diener et al., 2021; King et al., 2023; King and Christoffersen, 2024). These studies showed that the cumulative effects of dominant climate modes can explain a substantial fraction of multi-year to decadal

https://doi.org/10.5194/egusphere-2026-3461
Preprint. Discussion started: 8 July 2026

Antarctic ice-mass variability and can influence trends estimated over the GRACE/GRACE-FO era. Here we apply a multivariate regression framework previously used in Antarctica (King et al., 2023; King and Christoffersen, 2024) to Arctic glacier regions, focusing on NAO- and PDO-related climate variability. We test whether these two large-scale climate modes correspond to the leading interannual modes in the Arctic GIC gravimetry record, and how much the associated variability influences estimated regional mass-loss trends over the GRACE era.

2 Data and Methods

2.1 GRACE and GRACE-FO Glacier mass time series

We analysed Arctic-region glacier and ice cap (GIC) mass variability using time-variable gravity data from NASA/DLR's Gravity Recovery and Climate Experiment (GRACE) mission and GRACE Follow-On (GRACE-FO). Three distinct mascon solutions were adopted, provided by the Jet Propulsion Laboratory (JPL), the Goddard Space Flight Centre (GSFC), and the Centre for Space Research (CSR) at the University of Texas at Austin (Watkins et al., 2015; Wiese et al., 2016; Save et al., 2016; Loomis et al., 2019a). The study period spans April 2002 to October 2024. All mascon data applied include corrections for glacial isostatic adjustment using ICE-6G_D (Richard Peltier et al., 2018). They also include the low-degree corrections applied by the processing centres: degree-1 geocenter corrections following Sun et al. (2016), replacement of C_{20} with the TN-14 satellite-laser-ranging solution, and replacement of C_{30} with TN-14 (Loomis et al., 2020) from June 2018 for CSR and from August 2016 for GSFC and JPL. Missing monthly values within each mission were filled using linear interpolation, and all datasets were resampled to a uniform 0.5° × 0.5° grid. Three mascon solutions were then averaged to enhance robustness and suppress random noise.

GRACE and GRACE-FO observations provide a unique opportunity to assess glacier mass changes at global scales. However, GRACE mascons do not resolve mass change at the scale of exact glacier outlines. Although they are distributed on fine grids, their effective resolution is still several hundred kilometres, reflecting the band-limited GRACE observations and the regularization used in the mascon inversions (Loomis et al., 2019a; Save et al., 2016; Watkins et al., 2015). It poses challenges when resolving mass change in small or closely clustered glacierized regions (Jacob et al., 2012). These limitations are particularly pronounced in regions where the signal-to-noise ratio is low or where glacierized areas are adjacent to ice sheets, making signal separation difficult (Jacob et al., 2012). We found that some RGI-defined regions, such as Iceland (G06, Fig. S1) and parts of the Russian Arctic (G09, Fig. S1), are too small to be reliably resolved by GRACE mascon solutions. The signals over these regions tend to be spatially diffused, leading to potential underestimation if confined strictly within the RGI boundaries (Jacob et al., 2012). We used RGI v7.0 (Consortium, 2023; Maussion et al., 2023) outlines expanded by a 1° buffer (Ma et al., 2025) to reduce truncation of the spatially smoothed GRACE mascon signal over small or fragmented glacier regions. Sensitivity tests against independent altimetry-based mass-balance estimates indicated that a 1° land-only buffer gave the best overall agreement (Ma et al., 2025). Because the buffer was restricted to land, ocean mascon signals were not included. Land–ocean leakage corrections are already handled within the GRACE mascon products

https://doi.org/10.5194/egusphere-2026-3461
Preprint. Discussion started: 8 July 2026

used in this study. We compared the GRACE-derived mass trends for the seven Arctic glacier regions with previously published regional estimates from earlier studies. The results show that our Arctic regional mass balance estimates are consistent with the existing literature (Fig. S2).

We recognize the difficulty in separating signals from peripheral glacierized regions adjacent to ice sheets, particularly in Greenland and the Antarctic ice sheets (Jacob et al., 2012). In these areas, the GRACE signal integrates mass changes from both peripheral glaciers and the adjacent ice sheet margins, making attribution ambiguous (Jacob et al., 2012). We therefore excluded peripheral glacier regions whose signals could not be robustly separated from adjacent ice-sheet mass change, including the Greenland periphery and Antarctic peripheral sectors.

To reduce contamination of glacier mass signals by non-glacial terrestrial water storage (TWS), we corrected the GRACE/GRACE-FO regional mascon time series for the contribution of non-glacial terrestrial water storage variability using monthly hydrological fields from Global Land Data Assimilation System version 2.1 (GLDAS v2.1) (Rodell et al., 2004). This correction was applied consistently to all glacier regions, although it is particularly important in hydrologically complex regions such as High Mountain Asia (HMA) (Wouters et al., 2019; Ciracì et al., 2020; Loomis et al., 2019b; Wang et al., 2017; Matsuo and Heki, 2010). Glacierized grid cells were masked when constructing the correction to avoid unrealistically large, modeled water storage variations over ice-covered terrain.

To evaluate the sensitivity of the correction to hydrological model choice, we additionally considered the PCRaster Global Water Balance 2 model (Sutanudjaja et al., 2018) (PCR-GLOBWB 2) and the Community Land Model Version 5 (Lawrence et al., 2019) (CLM5.0) (Table S1). PCR-GLOBWB 2 provides terrestrial water-storage variations at 5 arcmin resolution and includes anthropogenic water-use effects not represented in GLDAS v2.1, whereas CLM5.0 provides an independent land-surface estimate with updated hydrology and snow physics. These products were not used as primary correction terms. Instead, they were used only to quantify hydrology-model dependence and to define an uncertainty benchmark. Hydrology-model dependence was quantified as the maximum absolute difference between the GLDAS-based correction trend and the alternative correction trends derived from PCR-GLOBWB 2 and CLM5.0. The final hydrological-correction uncertainty was computed as the quadrature sum of the GLDAS correction uncertainty and this model-spread term and was propagated into the regional mass balance uncertainties (Table S1).

The resulting GIC time series were then fitted using the following equation to remove the linear trend, semi-annual, and annual components.

$$y(t) = \alpha + \beta t + \sum_{k=1}^{k}[A_k \cos(2\pi\omega_k t) + B_k \sin(2\pi\omega_k t)] + \varepsilon(t)\ , \quad (1)$$

where $y(t)$ denotes the equivalent water height (EWH) anomaly at time t, α and β represent the intercept and linear trend, respectively, and $\varepsilon(t)$ is the residual term. The harmonic components represent cyclic variations with annual ($k = 1$) and semiannual ($k = 2$) frequencies. The coefficients A_k and B_k together capture the amplitude and phase of each harmonic component. The residuals were interpreted primarily as the interannual-to-decadal signal associated with glacier mass variability.

https://doi.org/10.5194/egusphere-2026-3461
Preprint. Discussion started: 8 July 2026

2.2 Climate indices

We focused on two climate modes that are known to influence atmospheric circulation, temperature, and precipitation over Arctic glacierized regions, the North Atlantic Oscillation (Ramos Buarque and Salas Y Melia, 2018; Bjørk et al., 2018) (NAO) and the Pacific Decadal Oscillation (Mantua et al., 1997; Papineau, 2001) (PDO). Monthly NAO and PDO index series were obtained from the NOAA/NCEI climate-monitoring archive.

We compared glacier-mass anomalies with cumulative forms of the NAO and PDO indices, following previous applications to ice-sheet SMB (Kim et al., 2020; King et al., 2023) and ice-shelf elevation change (Diener et al., 2021). For each monthly index, we first defined anomalies relative to a common 1971–1999 reference period, then truncated the series to the GRACE/GRACE-FO analysis window, normalized it (Fig. S3a, b), calculated the cumulative sum through time, and finally renormalized the resulting cumulative series (Fig. S3c, d). The resulting cumulative indices are denoted NAO_{Σ} and PDO_{Σ}. After detrending, these cumulative indices were used to compare with the detrended ICA components (Fig. S3e, f). We emphasize that NAO_{Σ} and PDO_{Σ} are used here to characterize multi-year climate variability (Mantua et al., 1997). This treatment is motivated by the expectation that persistent circulation anomalies may leave an integrated imprint on glacier mass anomalies (Bjørk et al., 2018; Ramos Buarque and Salas Y Melia, 2018; King et al., 2023).

To assess robustness to index construction, we compared the cumulative NAO and PDO indices with alternative representations of the same climate variability, including the corresponding raw monthly indices (Fig. S4). These tests show that the cumulative index representation is more closely associated with the glacier-mass modes than monthly fluctuations (Table S2).

2.3 Significance testing and temporal autocorrelation

Because cumulative climate indices enhance low-frequency variability and temporal autocorrelation, they reduce the effective degrees of freedom (DOF) and require autocorrelation-aware statistical testing (Chao and Chung, 2019; Williams et al., 2014). We evaluated the ICA-climate-index correlations using effective DOF adjustments and surrogate Monte Carlo tests based on 10000 pairs of independent AR(1) realizations (Chao and Chung, 2019; Williams et al., 2014) with the same missing data structures as the observed series. Correlations were evaluated over the full GRACE/GRACE-FO period and separately for the pre-gap and post-gap segments, with segment-wise differences assessed using Fisher-*z* tests. Results are reported in Tables S2 and S3.

2.4 Annual balance and seasonal contributions

Annual balances were defined from March of one year to March of the following year, so as to encompass the full melt season within a single balance year (Sasgen et al., 2022). For each region, the seasonal analysis was based on 19 valid annual-balance years after excluding years affected by the GRACE/GRACE-FO mission gap (Fig. S5). The annual balance was partitioned into a summer contribution (March–September) and a winter contribution (September–March of the

https://doi.org/10.5194/egusphere-2026-3461
Preprint. Discussion started: 8 July 2026

following year), such that the two seasonal terms sum exactly to the annual balance. To quantify the relative importance of seasonal mass changes for annual balance, we calculated the correlations of annual balance with the summer and winter contributions and summarized their relative influence using a seasonal dominance index defined as $D_2 = r(B,S)^2 - r(B,W)^2$, where B is annual balance, S is the summer contribution, and W is the winter contribution. Positive values indicate summer dominance and negative values indicate winter dominance (Fig. S5i).

2.5 Atmospheric and oceanic fields

Monthly atmospheric and oceanic fields were taken from the ERA5 reanalysis. From ERA5, we analysed mean sea-level pressure, 10 m winds, 2 m air temperature, sea-surface temperature, 700-hPa air temperature, total precipitation, and vertically integrated northward heat flux. Monthly anomalies were computed relative to the 1971–1999 climatology at each grid point. The fields were then restricted to 2002–2024 for comparison with the GRACE/GRACE-FO record. For cumulative-field analyses, anomaly fields were normalized, cumulatively summed, and renormalized before being regressed onto NAO_{Σ} and PDO_{Σ}. Seasonal-mean fields were used to examine the regional climate pathways linking wind, temperature, precipitation, and vertically integrated northward heat flux to annual glacier mass balance.

2.6 Correlation and regression analyses of atmospheric variables and mass balance

To diagnose the atmospheric conditions associated with glacier mass balance variability, we analysed June–August (JJA) and December–February (DJF) mean fields on a grid-point basis. Monthly fields were first referenced to the 1971–1999 climatology and then averaged to form seasonal anomalies. For scalar variables, we calculated lag-zero grid-point Pearson correlations with annual balance and its seasonal contributions. Significance was assessed using a two-sided Student's t test at the 5% level, with the effective DOF adjusted for autocorrelation. Significant areas are indicated in the figures by yellow contours (Figs. S7–S8, S10–S12). For wind fields, we estimated grid-point linear regressions of the zonal and meridional wind components against the corresponding mass balance series, so that the regression coefficients describe the associated anomalous circulation pattern (Figs. S6 and S9).

2.7 ICA analysis

Independent Component Analysis (ICA) has been demonstrated to be an effective tool for extracting geophysical signals from observed time series (Forootan and Kusche, 2012; Boergens et al., 2014; Liu et al., 2018). In this study, we applied ICA to isolate the dominant interannual glacier mass variability from GRACE/GRACE-FO mascon time series for GICs. Regional GIC time series were treated as mixtures of a smaller number of statistically independent source signals, and the separation was performed using the Fast-ICA algorithm (Hyvärinen, 1999) (Fig. S13). We first applied principal component analysis (PCA) to the regional GRACE mass anomaly fields to reduce dimensionality and then applied ICA to the retained PCs. Retaining five PCs in the main analysis was motivated by the scree structure (Fig. S14) and by the weak, spatially

https://doi.org/10.5194/egusphere-2026-3461
Preprint. Discussion started: 8 July 2026

incoherent variance contained in higher-order components. Higher-order ICs (IC3–IC5) each explained only a small fraction of the variance and were therefore not considered further (Fig. S15).

The ICA decomposition is written as

$$X(t) = B^{-1}Y(t) = WY(t)\,, \tag{2}$$

where $X(t)$ denotes the observed GIC mass change time series, B is the mixing matrix, $W = B^{-1}$ is the unmixing matrix and $Y(t)$ represents the estimated ICs. The rows of Y correspond to the ICs derived from ICA, while the column vectors of the unmixing matrix W represent the spatial modes associated with each IC. The contribution of the kth ICA mode to the original signal is

$$GRACE_{ICk} = y_k w_k\,, \tag{3}$$

where y_k is the temporal IC and w_k is the corresponding spatial mode. Because ICA solutions have arbitrary scaling, each spatial mode was normalized by its maximum absolute value and the corresponding temporal IC was multiplied by the same factor, so that their product retained the original units of X. The resulting $GRACE_{IC}$ fields were subsequently averaged over the spatial domain to obtain representative time series.

To assess sensitivity to the prescribed number of ICA sources, we repeated the decomposition with 3–10 components (Fig. S16). The first two components from the 3-component solution were taken as reference modes. For each m-component solution ($m = 4, \ldots, 10$), the component best matching each reference mode was identified by maximizing a stability index that combined temporal and spatial similarity, with one-to-one matching enforced between reference and candidate modes. Temporal similarity was measured using the absolute Pearson correlation coefficient,

$$\mathrm{corr}_k^{(m)} = \left|\mathrm{corr}\left(s_k^{\mathrm{ref}}(t), s_j^{(m)}(t)\right)\right|\,, \tag{4}$$

where $s_k^{\mathrm{ref}}(t)$ is the time series of the kth reference mode from the 3-component solution and $s_j^{(m)}(t)$ is the time series of the jth candidate mode from the m-component solution. Spatial similarity was measured using the absolute Tucker congruence coefficient, for which values close to 1 indicate highly similar patterns and values above about 0.95 are commonly interpreted as near-equivalent (Lorenzo-Seva and Ten Berge, 2006)

$$\emptyset_k^{(m)} = \left|\frac{\left(a_k^{\mathrm{ref}}\right)^{\mathrm{T}} a_j^{(m)}}{\sqrt{\left(a_k^{\mathrm{ref}}\right)^{\mathrm{T}} a_k^{\mathrm{ref}}}\sqrt{\left(a_j^{(m)}\right)^{\mathrm{T}} a_j^{(m)}}}\right|\,, \tag{5}$$

where a_k^{ref} and $a_j^{(m)}$ are the corresponding reference and candidate spatial modes. We then defined the stability index as

$$\mathrm{SI}_k^{(m)} = \mathrm{corr}_k^{(m)} \times \emptyset_k^{(m)}\,, \tag{6}$$

https://doi.org/10.5194/egusphere-2026-3461
Preprint. Discussion started: 8 July 2026

Under this test, the first ICA mode remained highly stable across 4–10 component solutions, with |corr| = 0.84–0.96, $|\phi|$ = 0.99–1.00, and SI= 0.83–0.96, whereas the second mode remained identifiable but was less stable, with |corr| = 0.73–0.93, $|\phi|$ = 0.76–0.88, and SI = 0.56–0.82 (Fig. S16). The 5-component solution showed agreement with the reference solution for the second mode, supporting the interpretation that the leading two ICA modes, especially the first mode, are robust features of the GRACE/GRACE-FO residual variability rather than artifacts of a specific choice of component number.

2.8 Multiple regression and trend-uncertainty estimation

We estimated the coefficients a, b, c, d and e of the functional model describing the time-evolving mass M at each time step t_i using ordinary least squares regression.

$$M(t_i) = a + b(t_i - t_0) + \sum_{k=1}^{2}\left(c_k^s \sin(2\pi f_k t_i) + c_k^c \cos(2\pi f_k t_i)\right) + d\,\mathrm{NAO}_\Sigma + e\,\mathrm{PDO}_\Sigma\,, \quad (7)$$

where $f_k = [1,2]$ cycles per year. Separate periodic coefficients were estimated for each of GRACE and GRACE-FO. We adopted t_0 as the midpoint of the GRACE series. To compare with trends estimated without climate-index terms, we also repeated the regression after removing the final two terms of Eq. (7).

GRACE-derived glacier mass time series contain pronounced low-frequency variability (King et al., 2023; Williams et al., 2014), and this must be accounted for when estimating regression-parameter uncertainties. For the regression without climate-index terms (Eq. (1)), residuals retained strong power at the lowest frequencies, so we estimated trend uncertainties using Hector with a power-law plus white-noise model (Bos et al., 2013). This increased the regional trend uncertainties by a mean factor of 10.2 relative to white-noise-only estimates (Table S4). In the regression including NAO_Σ and PDO_Σ, the linear trend and cumulative climate-index terms were solved simultaneously (Eq. (7)). This regression explained much of the lowest-frequency structure in the GRACE time series, leaving residuals whose temporal correlation was adequately represented by an AR(1) model. We therefore estimated the trend uncertainty from the full regression covariance under an AR(1) residual-noise model, which increased the white-noise uncertainties by a mean factor of 3.2 (Table S5).

The inclusion of NAO_Σ and PDO_Σ has two opposing effects on trend uncertainty. It reduces the low-frequency power remaining in the residuals, thereby reducing correlated-noise uncertainty, and it also introduces additional parameters that can covary with the linear trend, reducing precision through parameter trade-off. In the Arctic glacier regions, the reduction in residual low-frequency variability partly offsets the loss of precision from the additional climate-index terms, so the climate-index regression uncertainties are generally comparable to those from the raw power-law regression. This differs from cases where the additional climate-index terms dominate the uncertainty budget, and reflects the strong low-frequency variability present in the raw Arctic glacier mass series.

We combined these regression-parameter uncertainties with independent contributions from mascon errors and auxiliary corrections. GRACE uncertainties were propagated from the GSFC uncertainty fields, which provide spatially resolved estimates of mascon noise and leakage uncertainty. Following Loomis et al. (2019a), leakage uncertainty was separated into a stochastic leakage component and a deterministic leakage-trend component. For regional integrations, stochastic noise and

https://doi.org/10.5194/egusphere-2026-3461
Preprint. Discussion started: 8 July 2026

leakage terms were scaled by the effective number of independent mascons to account for spatial correlation among neighbouring mascons. The deterministic leakage-trend term was treated as a systematic component and was not reduced by spatial averaging.

Our regional mass time series are based on the mean of the JPL, CSR and GSFC mascon solutions. We also included a processing-centre uncertainty, defined from the spread of regional trends estimated independently from the three mascons. All mascon solutions used here already include a GIA correction. We included only the GIA model uncertainties reported by Jacob et al. (2012), Gardner et al. (2013) and Ciracì et al. (2020). For each regression model, the final regional trend uncertainty was computed as the quadrature sum of the correlated-noise regression uncertainty, noise uncertainty, leakage uncertainty, processing-centre spread, GIA uncertainty and hydrological-correction uncertainty (Table S6). All uncertainties are reported as 95% confidence intervals.

2.9 Regression against time-differenced GRACE data

In our analysis, we regressed undifferenced GRACE/GRACE-FO mass anomalies against cumulative climate indices, rather than differencing the gravimetry data and regressing against the corresponding raw monthly indices. In the absence of noise, the two formulations are closely related, as cumulatively summing the fitted terms from the differenced solution should reproduce the corresponding components of the undifferenced mass-anomaly series (King et al., 2023). However, time differencing amplifies high-frequency noise in GRACE/GRACE-FO data relative to the low-frequency signal, so the differenced formulation requires additional low-pass filtering.

To assess sensitivity to this methodological choice, we repeated the regression for three Arctic regions with pronounced climate variability: Alaska, Arctic Canada North and Svalbard (Fig. S17),

$$dM(t_i) = b(t_i - t_0) + \sum_{k=1}^{2}\left(c_k^s \sin(2\pi f_k t_i) + c_k^c \cos(2\pi f_k t_i)\right) + d\mathrm{NAO} + e\mathrm{PDO}\,, \quad (8)$$

where $dM(t_i)$ is the first-differenced GRACE/GRACE-FO mass anomaly series. Monthly GRACE/GRACE-FO mass anomalies were first-differenced. The NAO and PDO indices were smoothed using the same running-mean window as the differenced gravimetry series. After regression, the fitted climate-related terms were cumulatively summed to reconstruct a mass-like component for comparison with the climate-related component estimated from the undifferenced regression (Fig. S17c).

We evaluated running-mean windows from 13 to 55 months and selected the preferred window as that minimizing the absolute difference in cumulative climate-related mass change relative to the undifferenced solution (Table S7). In all three regions, a 25-month window gave the closest agreement. With this choice, the reconstructed climate-related component from the differenced solution showed agreement with the undifferenced solution, and the corresponding cumulative mass differences were +3%, −2% and +1%, respectively (Fig. S17). At longer windows, the inferred climate-related mass change became increasingly sensitive to the choice of smoothing. We therefore adopt the undifferenced regression against

https://doi.org/10.5194/egusphere-2026-3461
Preprint. Discussion started: 8 July 2026

cumulative indices in the main analysis, because it avoids the additional uncertainty introduced by low-pass filtering of differenced GRACE/GRACE-FO data.

2.10 Partial variance explained by NAO and PDO

We calculated the partial variance (R^2) of the GRACE time series explained by each, or by both, of the NAO_{Σ} and PDO_{Σ} components, where R^2 is defined as the square of the partial correlation coefficient (R). Partial correlation, unlike conventional correlation, allows the influence of other confounding variables, namely the linear trend, periodic components, and the alternative climate term (NAO_{Σ} or PDO_{Σ}, as appropriate), to be controlled.

3 Results

3.1 Independent spatiotemporal modes of detrended GRACE data

We applied ICA to detrended monthly mass anomaly time series from 17 Randolph Glacier Inventory (RGI)-based glacier regions in the global GRACE/GRACE-FO record over 2002–2024 (Figs. S18−S20). This spatiotemporal decomposition revealed two dominant modes that together explain 70% of the interannual variance in the global GIC record (Fig. S19). Their spatial modes (Global Modes 1 and 2) show marked heterogeneity, with the interannual signals concentrated in the Arctic (Fig. S19).

To isolate Arctic-specific variability, we performed a separate ICA on Arctic GICs, defined here as Alaska (ALA), Arctic Canada North (ACN), Arctic Canada South (ACS), Iceland (ICE), Svalbard (SVA), Scandinavia (SCA) and the Russian Arctic (RA, RGI regions G01, G03, G04, G06–G09). Two dominant modes were identified, together explaining 75% of the variance in the detrended Arctic GIC time series (Fig. 1a, b). Notably, the two Arctic components (Arctic IC1–IC2) closely resemble their global counterparts (Global IC1–IC2) in both temporal evolution and spatial patterns.

We compared the leading Arctic ICA components with the cumulative NAO and PDO climate indices (Fig. 1c, d and Fig. S3). Over the GRACE/GRACE-FO period, both cumulative indices exhibit downward trends (Fig. S3c, d). After detrending, they show pronounced interannual-to-decadal variability (Fig. S3e, f). Comparison with the Arctic ICs shows close agreement between NAO_{Σ} and Arctic IC1 (Fig. 1c, $r = -0.84$) and between PDO_{Σ} and Arctic IC2 (Fig. 1d, $r = 0.85$). These close agreements suggest that recent interannual-to-decadal Arctic glacier-mass variability is related to both NAO- and PDO-associated climate variability.

https://doi.org/10.5194/egusphere-2026-3461
Preprint. Discussion started: 8 July 2026

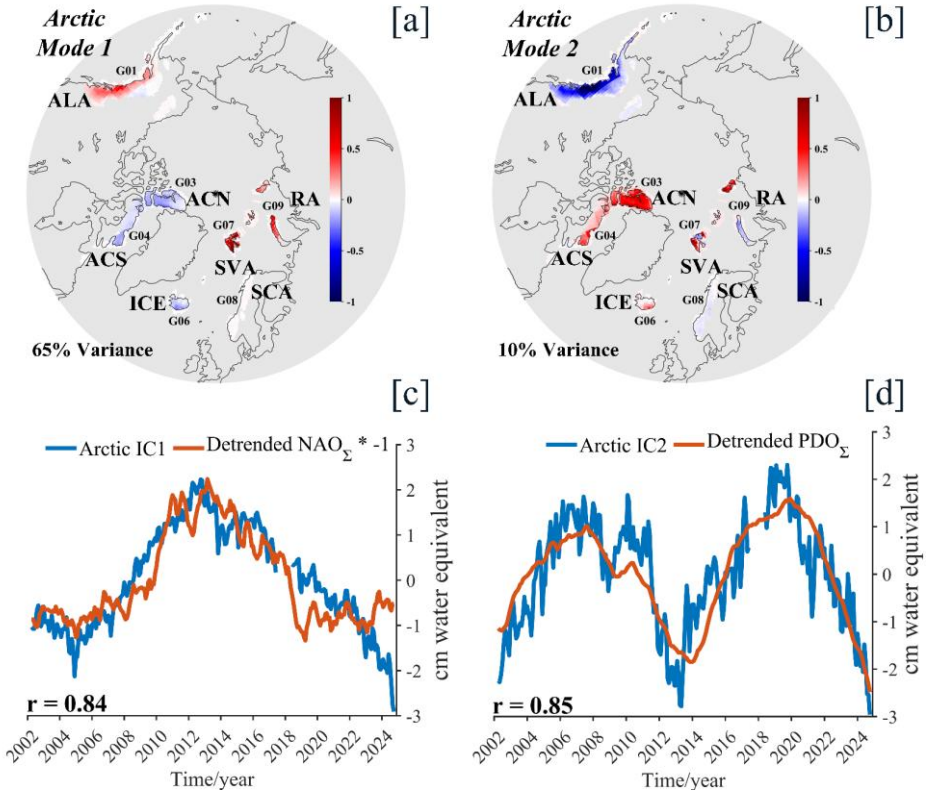

Figure 1: Leading independent modes of Arctic glacier mass variability. a, b, Spatial patterns of the first two ICA modes (Arctic Mode 1 and Arctic Mode 2) derived from detrended GRACE/GRACE-FO mass anomaly time series for Arctic GICs across seven regions, explaining 65% (a, c) and 10% (b, d) of the interannual variance, respectively. c, d, Corresponding independent components IC1 and IC2 (blue) shown together with the detrended NAO$_\Sigma$ (c) and PDO$_\Sigma$ (d) indices (orange). All time series are normalised over 2002–2024. The secondary modes are presented in Fig. S15.

Considering the Arctic Mode/IC pairs, both modes exhibit a coherent pattern of spatial co-variability across the Arctic. ACN (G03), ACS (G04) and ICE (G06) evolve largely in phase with one another, while ALA (G01) tends to vary in the opposite sense; SVA (G07), SCA (G08) and RA (G09) cluster with ALA in Arctic Mode 1, but reverse sign relative to ALA in Arctic Mode 2 (Fig. 1a, b).

3.2 NAO–linked zonal co-variability in Arctic ice mass variability

ICA provides data-driven spatial weights for each mode (Eq. (2)), allowing us to map how NAO-related variability is expressed in regional glacier-mass anomalies (Fig. 2). We partition the Arctic glacier regions into a western sector (G03, G04, G06) and an eastern sector (G01, G07, G08, G09). In the western sector, anomalies tend to be positive during intervals of increasing NAO$_\Sigma$ and negative during intervals of decreasing NAO$_\Sigma$, whereas the eastern sector shows the opposite pattern. The summed anomalies highlight a marked asymmetry: positive anomalies in the western sector (+177 Gt) slightly exceed negative ones (–133 Gt), whereas in the eastern sector, negative anomalies (–388 Gt) outweigh positive anomalies (+290 Gt).

https://doi.org/10.5194/egusphere-2026-3461
Preprint. Discussion started: 8 July 2026

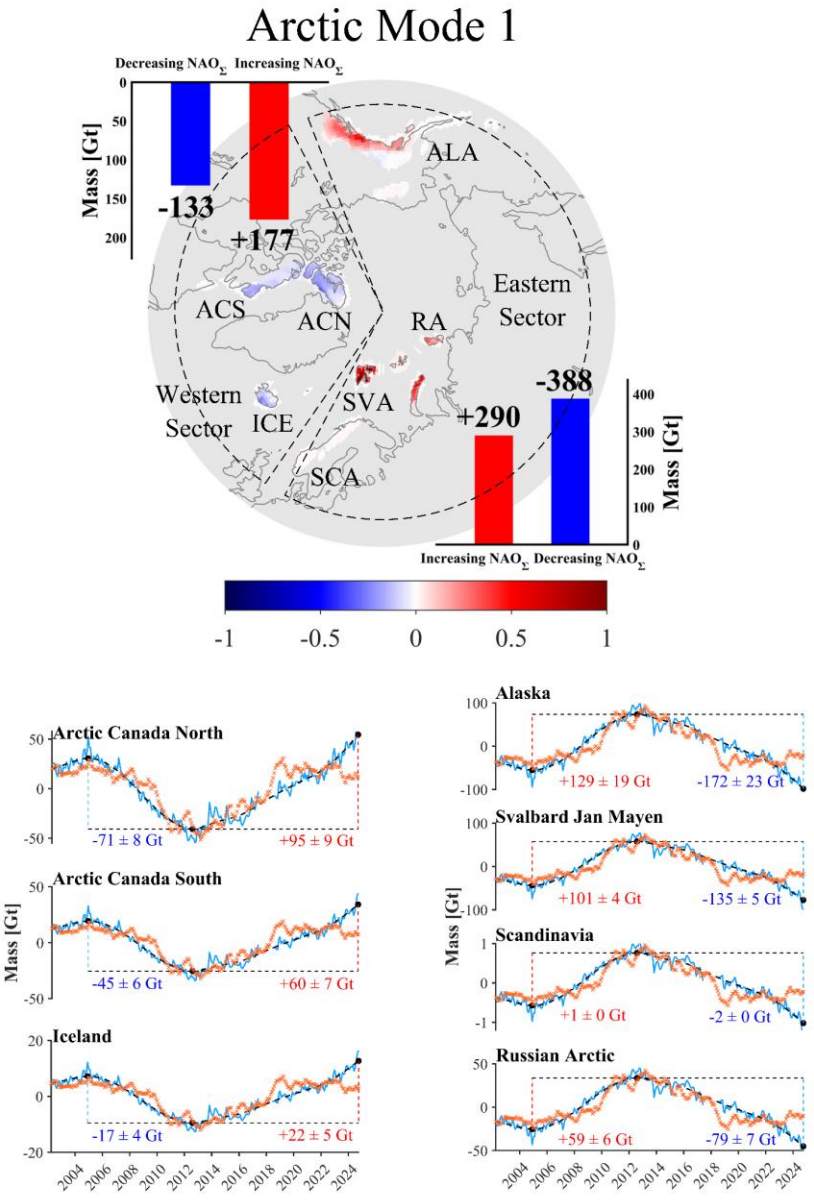

Figure 2: Spatial pattern of Arctic Mode 1. Delineated into two subregions based on the NAO-related mode: the Western Sector (G03, G04, G06) and the Eastern Sector (G01, G07, G08, G09). Bar plots show the summed positive and negative interannual mass anomalies in each sector during intervals of increasing and decreasing NAO$_\Sigma$ anomalies. The lower panels illustrate interannual mass anomaly variations for selected subregions, with the left subpanels representing the Western Sector and the right subpanels representing the Eastern Sector. The blue curves denote the regional mass variations associated with Arctic IC1, calculated from Eq. (3). The black dashed lines are smoothed versions of the blue lines, applying a Hodrick–Prescott low-pass filter (Hodrick and Prescott, 1997). The red and blue dashed lines indicate the maximum mass differences before and after 2013, referenced to the lowest (left) or highest (right) values within the study period. The orange crosses denote the fitted NAO$_\Sigma$ contribution from the regional regression model.

https://doi.org/10.5194/egusphere-2026-3461
Preprint. Discussion started: 8 July 2026

3.3 PDO–linked annular heterogeneity of Arctic ice mass variability

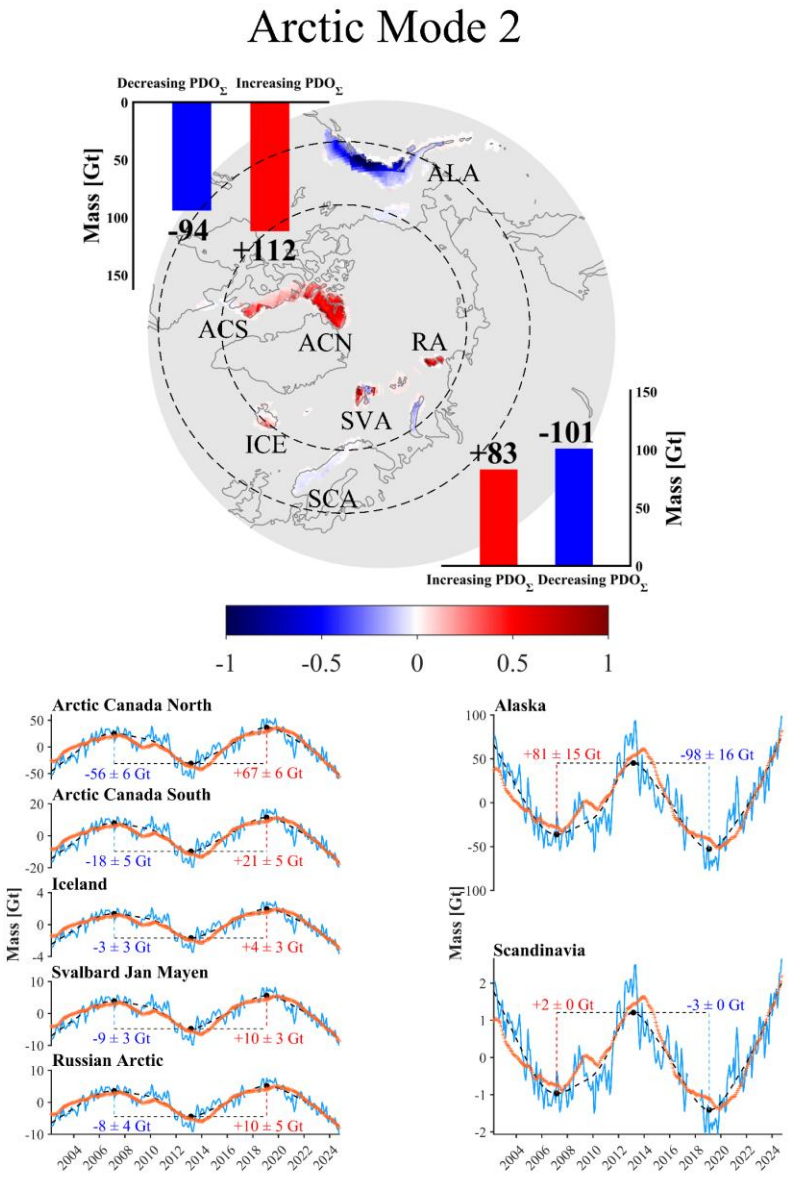

Figure 3: Spatial pattern of Arctic Mode 2. Classified based on the PDO-related mode into the Central Arctic Zone (G03, G04, G06, G07, G09) and the Peripheral Zone (G01, G08). Bar plots show the summed positive and negative interannual mass anomalies in both zones during intervals of increasing and decreasing PDO$_\Sigma$ anomalies. The lower panels show interannual mass anomaly variations for selected regions, with those in the Peripheral Zone displayed on the left and those in the Central Arctic on the right. The blue curves represent regional mass variations associated with Arctic IC2, calculated from Eq. (3). The black dashed lines are smoothed versions of the blue lines, applying a Hodrick–Prescott low-pass filter (Hodrick and Prescott, 1997). The red and blue dashed lines mark the maximum mass differences before and after 2013, referenced to the highest (right) or lowest (left) values over the study period. The orange crosses denote the fitted PDO$_\Sigma$ contribution from the regional regression model.

https://doi.org/10.5194/egusphere-2026-3461
Preprint. Discussion started: 8 July 2026

Arctic Mode 2 is associated with PDO-related interannual variability (Fig. 3). Based on its spatial pattern, we subdivide the Arctic into a central Arctic zone (G03, G04, G06, G07, G09) and an outer peripheral zone (G01, G08). In the central zone, anomalies tend to be positive during intervals of increasing PDO_{Σ} and negative during intervals of decreasing PDO_{Σ}. The peripheral zone exhibits the opposite behaviour, with negative anomalies during increasing PDO_{Σ} and positive anomalies during decreasing PDO_{Σ}. In the central Arctic zone, months with positive anomalies sum to +112 Gt, exceeding the –94 Gt summed over months with negative anomalies; in the periphery zone, ALA (G01) alone contributes +83 Gt during decreasing PDO_{Σ} intervals and –101 Gt during increasing PDO_{Σ} intervals.

Given that the GRACE/GRACE-FO time series spans only just over two decades, the presence of pronounced interannual-to-decadal variability means that estimated trends will be sensitive to whether and how that variability is handled in time-series analyses (King et al., 2023). The preceding ICA analysis provides a data-driven means of identifying dominant modes of variability in the GRACE/GRACE-FO record. Following ref.(King et al., 2023), we used a regression framework that incorporates the NAO_{Σ} and PDO_{Σ} to quantify their contributions to glacier mass variability.

3.4 Multiple linear regression of GRACE-derived glacier mass change trends

We regressed the seven regional GRACE mass-anomaly time series against a linear, annual and semi-annual harmonics, and PDO_{Σ} and NAO_{Σ} terms (Eq. (7)). No trends were removed from either the GRACE data or the cumulative indices before the regression (Fig. S3c, d). Thus, the linear trend and the contributions associated with PDO_{Σ} and NAO_{Σ} were estimated simultaneously. We then computed the partial variance (R^2) explained by the PDO_{Σ} and NAO_{Σ} terms, accounting for the other regression terms, including the linear trend (Fig. S21).

In Alaska (Fig. S21a), the PDO_{Σ} and NAO_{Σ} together explain 57.0% of interannual variability, with NAO_{Σ} being the dominant contributor. In Arctic Canada North (Fig. S21b), NAO_{Σ} accounts for most of the explained variance (approximately 43%) and is negatively correlated with GRACE anomalies. Arctic Canada South and Iceland (Fig. S21c, d) show similar NAO-dominated behaviour (approximately 38–40%), while PDO_{Σ} contributes only marginally. In Svalbard and Russian Arctic (Fig. S21e, g), NAO_{Σ} again dominates (approximately 65–77%), with PDO_{Σ} exerting a weaker, opposite-signed influence. In Scandinavia (Fig. S21f), neither index plays a significant role.

3.5 The impact of interannual-to-decadal variability on glacier long-term trends

Our regression allows partitioning of GRACE/GRACE-FO glacier-mass trends into a residual linear term and components associated with NAO_{Σ} and PDO_{Σ}. We interpret the residual linear term as representing glacier-mass changes associated with forcing before and/or during the data period, together with longer-term variability not captured by the NAO_{Σ} and PDO_{Σ} terms. Because the NAO and PDO indices are, on average, negative relative to the reference period during 2002–2024, their cumulative sums show downward trends (Figs. S3c, d). In the regression, these cumulative-index trends contribute mass-

https://doi.org/10.5194/egusphere-2026-3461
Preprint. Discussion started: 8 July 2026

change trends. The magnitudes of these contributions depend on the fitted response to the non-linear parts of NAO_{Σ} and PDO_{Σ} (Figs. S3e, f), indicating that multi-year departures associated with persistent negative NAO/PDO phases project onto regional glacier-mass trends.

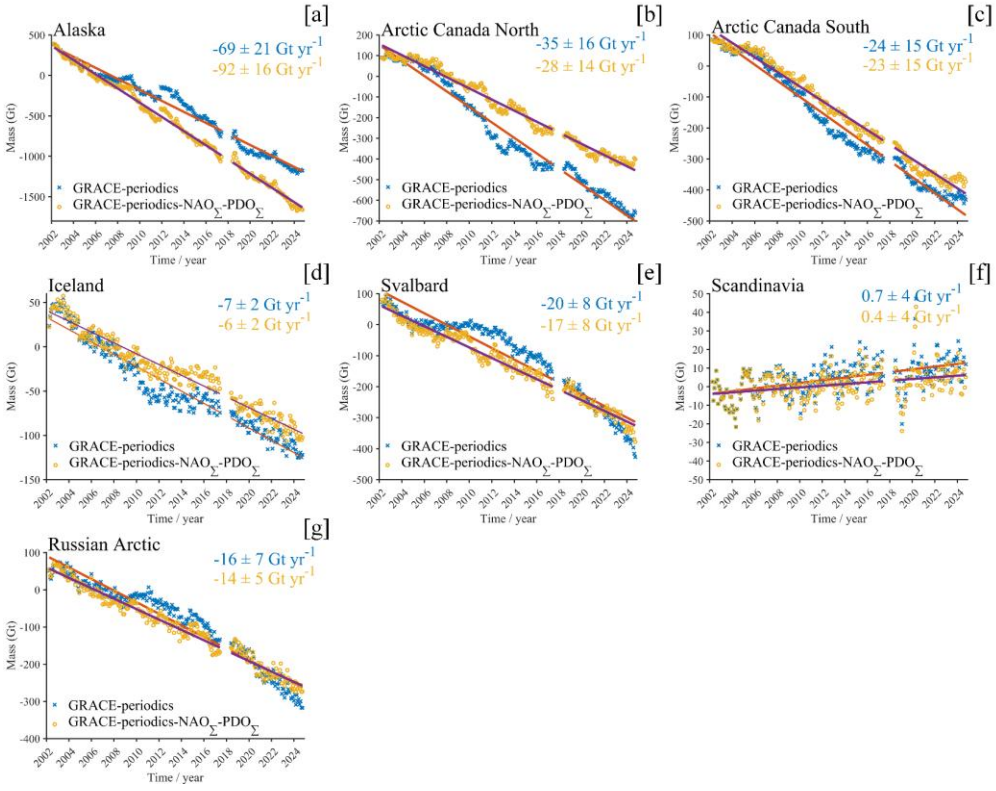

Figure 4: Linear trends in Arctic glacier mass change derived from GRACE. Linear trends for ALA, ACN, ACS, ICE, SVA, SCA, and RA are shown, estimated from regressions that include (blue) and exclude (orange) the NAO_{Σ} and PDO_{Σ} components.

In Alaska, the largest mass-loss sector in the Arctic, the unadjusted linear trend is –69 ± 21 Gt yr^{-1}. Removing NAO_{Σ} and PDO_{Σ}, the corrected linear trend of –92 ± 16 Gt yr^{-1} (Fig. 4a), using the 1971–1999 reference period. The NAO_{Σ} and PDO_{Σ} terms contribute +23 Gt yr^{-1} to the trend, making the unadjusted GRACE/GRACE-FO trend 25% less negative than the residual trend.

In Arctic Canada North, the sign of this effect is reversed (Fig. 4b). The unadjusted trend is –35 ± 16 Gt yr^{-1}, whereas removing NAO_{Σ} and PDO_{Σ}, the corrected trend of –28 ± 14 Gt yr^{-1}. The climate mode terms contribute a net positive tendency of –7 Gt yr^{-1}. These results show that interannual-to-decadal variability can influence estimated GRACE/GRACE-FO trends in opposite directions across Arctic glacier regions.

Repeating the climate-index regression with NAO_{Σ} and PDO_{Σ} referenced to 1981–2010 and 1991–2020 gives the same regional interpretation (Fig. S22). In Alaska, the residual linear trends remain more negative than the trend inferred without

https://doi.org/10.5194/egusphere-2026-3461
Preprint. Discussion started: 8 July 2026

the climate-index terms (Fig. 4a and Fig. S22c). Thus, the choice of reference period does not affect the quantitative partitioning of the NAO_{Σ}- and PDO_{Σ}-related trend contribution or the main regional interpretation.

4 Discussion

4.1 Arctic circulation modes

Regression maps of sea-level pressure (SLP), wind and associated surface-climate anomalies suggest that the two ICA modes correspond to distinct expressions of Arctic circulation variability rather than to a spatially uniform Arctic response (Figs. S23, S24). The NAO_{Σ}-related pattern is broadly consistent with enhanced meridional exchange between the North Atlantic and the eastern Arctic, whereas the PDO_{Σ}-related pattern points to a Pacific-sector pathway expressed most clearly in Alaska and nearby Arctic regions.

These circulation structures imply a west–east redistribution of heat and moisture across the Arctic, helping to explain why neighbouring glacier regions can exhibit contrasting mass balance anomalies over the same period (Bjørk et al., 2018; Sasgen et al., 2022). This is consistent with earlier work suggesting that Arctic climate variability can be organized by persistent large-scale circulation regimes that redistribute heat, moisture and freshwater across the Arctic system over multi-year timescales (Proshutinsky et al., 2015).

Using unsummed NAO and PDO indices with wind data (Fig. S25), NAO-related anomalies are concentrated over the Canadian Arctic and extend across the Arctic in winter, when east–west pressure gradients and meridional exchanges between the North Atlantic and Arctic sectors are strongest (Figs. S25e and S27). Together with the cumulative-index regressions, this indicates that sustained meridional circulation are an important part of the NAO-related Arctic circulation, potentially affecting winter moisture transport and the regional mass-balance response. PDO-related anomalies are more regional, centred on the North Pacific–Alaska sector and amplified in winter (Fig. S25f). Near-surface temperature anomalies mirror these patterns, including a winter-strengthened NAO contrast between the Canadian Arctic and the Eurasian Arctic, and a PDO-related anomaly over Alaska and adjacent Pacific Arctic regions (Fig. S26).

The ~25% change in the Alaska trend estimates after including NAO_{Σ} and PDO_{Σ} provides a regional example (Fig. 4a). For NAO, such sustained departures are consistent with documented decadal-scale persistence of NAO phase and associated changes in winter circulation, temperature and moisture transport across the North Atlantic–Arctic sector (Hurrell, 1995; Visbeck et al., 2001). Recent winter NAO trends have been interpreted as arising from internal variability amplified by, or combined with, a contribution from increasing greenhouse-gas concentrations (Gillett et al., 2003). PDO variability is different, being viewed as interannual-to-decadal North Pacific variability arising from coupled tropical and extratropical processes, with apparent regime-like shifts (Newman et al., 2016; Mantua et al., 1997). Thus, the trend differences reflect the projection of sustained NAO- and PDO-related circulation anomalies onto regional glacier mass change.

https://doi.org/10.5194/egusphere-2026-3461
Preprint. Discussion started: 8 July 2026

4.2 Physical links between circulation and glacier mass variability

These circulation anomalies are expressed through seasonally distinct surface-mass-balance pathways (Ramos Buarque and Salas Y Melia, 2018). The cold-season signal is associated with coherent DJF SLP, wind, and precipitation anomalies, consistent with circulation-controlled moisture transport and snowfall accumulation (Figs. S6–S8). The warm-season signal is associated with JJA SLP, wind, northward heat flux, and near-surface temperature anomalies, consistent with melt-favouring summer conditions (Figs. S9–S12) (Ramos Buarque and Salas Y Melia, 2018; Bjørk et al., 2018; Sasgen et al., 2022). These seasonal diagnostics provide a physically consistent framework linking the NAO_{Σ} and PDO_{Σ} modes to annual glacier-mass anomalies. Arctic Canada North (ACN) provides the clearest summer-dominated annual balance signal (S9b–S12b, S5b and S5i). By contrast, Svalbard (SVA) retains mixed seasonal pattern, indicating that its annual balance integrates both winter mass gain and summer ablation (Fig. S5e, i).

The seasonal contributions vary across the Arctic. In Alaska, both seasonal terms contribute to annual balance, with the cold-season contribution being stronger (Fig. S5a, h and i). At the same time, Alaska exhibits a distinct warm-season circulation, heat-flux and temperature signature, consistent with a Pacific-sector pathway and with the PDO-related influence inferred from the regression analysis (Figs. S9a–S12a) (Papineau, 2001). Most Arctic regions show mixed seasonal control (Fig. S5). These regionally varying seasonal contributions provide a physical explanation for how NAO- and PDO-related climate variability can influence glacier mass changes.

4.3 Limitations

The main limitation is that the IC1-NAO_{Σ} relationship weakens after ~2018 (Tables S1 and S2). This likely reflects non-stationarity in the NAO-related circulation influence or multiple processes are captured by the ICA. Such behaviour is plausible given the strong regional and seasonal dependence of North Atlantic circulation influences on glacier mass balance in Svalbard and Arctic Canada (Sasgen et al., 2022; Bonan et al., 2019). The short post-gap record limits further diagnosis. Importantly, these limitations do not alter the central conclusion that multi-year climate variability influences glacier mass variability and can project onto trend estimates over short observational periods. Rather, they indicate that the magnitude and expression of this effect may vary over time, reinforcing the need to explicitly account for evolving climate variability when interpreting recent glacier mass change (Proshutinsky et al., 2015).

5 Conclusion

Our findings show that the leading interannual-to-decadal variability resolved in the GRACE/GRACE-FO global glacier record is dominated by Arctic glacier regions and covaries with NAO- and PDO-related climate variability, with direct consequences for how short gravimetry records are interpreted. Accounting for this variability materially changes the fitted trends inferred from the GRACE/GRACE-FO record across Arctic glacier regions. Alaska provides the clearest example:

https://doi.org/10.5194/egusphere-2026-3461
Preprint. Discussion started: 8 July 2026

accounting for NAO- and PDO-related variability makes the estimated trend about 33% more negative than that derived from the gravimetry record. Accounting for the same variability in Arctic Canada North, by contrast, makes the fitted trend over the GRACE/GRACE-FO period less negative.

These regional contrasts show that trend estimates derived from records spanning only about two decades can differ substantially depending on the duration and magnitude to which modes of climate variability stay in a particular phase. The PDO-related component is consistent with internal North Pacific variability, whereas the NAO-related component may also include a forced contribution through recent changes in winter North Atlantic circulation. Future changes in the persistence of these climate modes may influence the regional pattern and timing of Arctic glacier mass loss, provided that the relationships identified here persist under continued warming.

Code availability

Code used to analyse the data and prepare figures will be made available upon request.

Data availability

All underlying data are openly available.

CSR Mascon: http://www2.csr.utexas.edu/grace/RL06_mascons.html

GSFC Mascon: https://earth.gsfc.nasa.gov/geo/data/grace-mascons

JPL Mascon: https://grace.jpl.nasa.gov/data/get-data/jpl_global_mascons

GIC data: https://doi.org/10.6084/m9.figshare.30521018

NAO Indices: https://www.ncei.noaa.gov/access/monitoring/nao/

PDO Indices: https://www.ncei.noaa.gov/access/monitoring/pdo/

ERA5 data: https://www.ecmwf.int/en/forecasts/datasets/reanalysis-datasets/era5

Coastlines: https://www.ngdc.noaa.gov/mgg/shorelines/data/gshhg/latest/

Author contributions

Q.W. and X.M. conceived the study. X.M. conducted the analysis and wrote the manuscript. M.A.K., J.B. and Q.W. contributed significantly to study design and provided critical feedback on the methodology and interpretation. B.L. contributed to GIC time series decomposition and statistical analysis. W.S. assisted with the interpretation. All authors contributed to manuscript review.

https://doi.org/10.5194/egusphere-2026-3461
Preprint. Discussion started: 8 July 2026

Competing interests

The authors declare that they have no conflict of interest.

Acknowledgements and Financial support

This work was financial supported by National Natural Science Foundation of China (42474007, 42104010, 42174097, 41974093, 41774088 and 41904003), and the Fundamental Research Funds for the Central Universities. This work was supported by the Australian Research Council (ARC; https://ror.org/05mmh0f86) Special Research Initiative, Australian Centre for Excellence in Antarctic Science (Project ID SR200100008), and an ARC Laureate Fellowship (Project ID FL250100022), by the Technical University of Munich – Institute for Advanced Study, Germany and European Union's Horizon 2020 research and 459 innovation programme through the project Arctic PASSION (grant number: 101003472). We extend our gratitude to the Centre for Space Research (CSR), Goddard Space Flight Centre (GSFC), and Jet Propulsion Laboratory (JPL) for providing the GRACE mascon solutions.

References

Arendt, A., Walsh, J., and Harrison, W.: Changes of Glaciers and Climate in Northwestern North America during the Late Twentieth Century, Journal of Climate, 22, 4117-4134, https://doi.org/10.1175/2009JCLI2784.1, 2009.

Bamber, J. L., Westaway, R. M., Marzeion, B., and Wouters, B.: The land ice contribution to sea level during the satellite era, Environmental Research Letters, 13, 063008, https://doi.org/10.1088/1748-9326/aac2f0, 2018.

Bjørk, A. A., Aagaard, S., Lütt, A., Khan, S. A., Box, J. E., Kjeldsen, K. K., Larsen, N. K., Korsgaard, N. J., Cappelen, J., Colgan, W. T., Machguth, H., Andresen, C. S., Peings, Y., and Kjær, K. H.: Changes in Greenland's peripheral glaciers linked to the North Atlantic Oscillation, Nature Climate Change, 8, 48–52, https://doi.org/10.1038/s41558-017-0029-1, 2018.

Boergens, E., Rangelova, E., Sideris, M. G., and Kusche, J.: Assessment of the capabilities of the temporal and spatiotemporal ICA method for geophysical signal separation in GRACE data, Journal of Geophysical Research-Solid Earth, 119, 4429-4447, https://doi.org/10.1002/2013jb010452, 2014.

Bolch, T., Sorensen, L. S., Simonsen, S. B., Mölg, N., Machguth, H., Rastner, P., and Paul, F.: Mass loss of Greenland's glaciers and ice caps 2003-2008 revealed from ICESat laser altimetry data, Geophysical Research Letters, 40, 875-881, https://doi.org/10.1002/grl.50270, 2013.

Bonan, D. B., Christian, J. E., and Christianson, K.: Influence of North Atlantic climate variability on glacier mass balance in Norway, Sweden and Svalbard, Journal of Glaciology, 65, 580-594, https://doi.org/10.1017/jog.2019.35, 2019.

Bos, M. S., Fernandes, R. M. S., Williams, S. D. P., and Bastos, L.: Fast error analysis of continuous GNSS observations with missing data, Journal of Geodesy, 87, 351-360, https://doi.org/10.1007/s00190-012-0605-0, 2013.

Box, J. E., Colgan, W. T., Wouters, B., Burgess, D. O., O'Neel, S., Thomson, L. I., and Mernild, S. H.: Global sea-level contribution from Arctic land ice: 1971-2017, Environmental Research Letters, 13, 125012, https://doi.org/10.1088/1748-9326/aaf2ed, 2018.

Chao, B. F. and Chung, C. H.: On Estimating the Cross Correlation and Least Squares Fit of One Data Set to Another With Time Shift, Earth and Space Science, 6, 1409-1415, https://doi.org/10.1029/2018ea000548, 2019.

Ciracì, E., Velicogna, I., and Sutterley, T. C.: Mass Balance of Novaya Zemlya Archipelago, Russian High Arctic, Using Time-Variable Gravity from GRACE and Altimetry Data from ICESat and CryoSat-2, Remote Sensing, 10, https://doi.org/10.3390/rs10111817, 2018.

https://doi.org/10.5194/egusphere-2026-3461
Preprint. Discussion started: 8 July 2026

Ciracì, E., Velicogna, I., and Swenson, S.: Continuity of the Mass Loss of the World's Glaciers and Ice Caps From the GRACE and GRACE Follow-On Missions, Geophysical Research Letters, 47, e2019GL086926, https://doi.org/10.1029/2019gl086926, 2020.

Consortium, R.: Randolph Glacier Inventory - A Dataset of Global Glacier Outlines, Version 7 [dataset], 10.5067/F6JMOVY5NAVZ, 2023.

Diener, T., Sasgen, I., Agosta, C., Fürst, J. J., Braun, M. H., Konrad, H., and Fettweis, X.: Acceleration of Dynamic Ice Loss in Antarctica From Satellite Gravimetry, Front. Earth Sci., 9, https://doi.org/10.3389/feart.2021.741789, 2021.

Dussaillant, I., Hugonnet, R., Huss, M., Berthier, E., Bannwart, J., Paul, F., and Zemp, M.: Annual mass change of the world's glaciers from 1976 to 2024 by temporal downscaling of satellite data with in situ observations, Earth System Science Data, 17, 1977-2006, https://doi.org/10.5194/essd-17-1977-2025, 2025.

Forootan, E. and Kusche, J.: Separation of global time-variable gravity signals into maximally independent components, Journal of Geodesy, 86, 477-497, https://doi.org/10.1007/s00190-011-0532-5, 2012.

Gardner, A. S., Moholdt, G., Cogley, J. G., Wouters, B., Arendt, A. A., Wahr, J., Berthier, E., Hock, R., Pfeffer, W. T., Kaser, G., Ligtenberg, S. R. M., Bolch, T., Sharp, M. J., Hagen, J. O., van den Broeke, M. R., and Paul, F.: A Reconciled Estimate of Glacier Contributions to Sea Level Rise: 2003 to 2009, Science, 340, 852-857, https://doi.org/10.1126/science.1234532, 2013.

Gillett, N. P., Graf, H. F., and Osborn, T.: Climate change and the North Atlantic oscillation, Geophysical Monograph-American Geophysical Union, 134, 193-210, https://doi.org/10.1029/134GM09, 2003.

Harig, C. and Simons, F. J.: Ice mass loss in Greenland, the Gulf of Alaska, and the Canadian Archipelago: Seasonal cycles and decadal trends, Geophysical Research Letters, 43, 3150-3159, https://doi.org/10.1002/2016gl067759, 2016.

Hock, R., Bliss, A., Marzeion, B., Giesen, R. H., Hirabayashi, Y., Huss, M., Radic, V., and Slangen, A. B. A.: GlacierMIP - A model intercomparison of global-scale glacier mass-balance models and projections, Journal of Glaciology, 65, 453-467, https://doi.org/10.1017/jog.2019.22, 2019.

Hodrick, R. J. and Prescott, E. C.: Postwar US business cycles: An empirical investigation, Journal of Money Credit and Banking, 29, 1-16, https://doi.org/10.2307/2953682, 1997.

Hugonnet, R., McNabb, R., Berthier, E., Menounos, B., Nuth, C., Girod, L., Farinotti, D., Huss, M., Dussaillant, I., Brun, F., and Kääb, A.: Accelerated global glacier mass loss in the early twenty-first century, Nature, 592, 726–731, https://doi.org/10.1038/s41586-021-03436-z, 2021.

Hurrell, J. W.: Decadal trends in the North Atlantic Oscillation: Regional temperatures and precipitation, Science, 269, 676-679, https://doi.org/10.1126/science.269.5224.676, 1995.

Hyvärinen, A.: Fast and robust fixed-point algorithms for independent component analysis, Ieee Transactions on Neural Networks, 10, 626-634, https://doi.org/10.1109/72.761722, 1999.

Jacob, T., Wahr, J., Pfeffer, W. T., and Swenson, S.: Recent contributions of glaciers and ice caps to sea level rise, Nature, 482, 514-518, https://doi.org/10.1038/nature10847, 2012.

Jakob, L. and Gourmelen, N.: Glacier Mass Loss Between 2010 and 2020 Dominated by Atmospheric Forcing, Geophysical Research Letters, 50, e2023GL102954, https://doi.org/10.1029/2023gl102954, 2023.

Jakob, L., Gourmelen, N., Ewart, M., and Plummer, S.: Spatially and temporally resolved ice loss in High Mountain Asia and the Gulf of Alaska observed by CryoSat-2 swath altimetry between 2010 and 2019, Cryosphere 15, 1845-1862, https://doi.org/10.5194/tc-15-1845-2021, 2021.

Kim, B. H., Seo, K. W., Eom, J., Chen, J. L., and Wilson, C. R.: Antarctic ice mass variations from 1979 to 2017 driven by anomalous precipitation accumulation, Scientific Reports, 10, 20366, https://doi.org/10.1038/s41598-020-77403-5, 2020.

King, M. A. and Christoffersen, P.: Major Modes of Climate Variability Dominate Nonlinear Antarctic Ice-Sheet Elevation Changes 2002-2020, Geophysical Research Letters, 51, e2024GL108844, https://doi.org/10.1029/2024gl108844, 2024.

King, M. A., Lyu, K., and Zhang, X. B.: Climate variability a key driver of recent Antarctic ice-mass change, Nature Geoscience, 16, 1128–1135, https://doi.org/10.1038/s41561-023-01317-w, 2023.

King, M. A., Bingham, R. J., Moore, P., Whitehouse, P. L., Bentley, M. J., and Milne, G. A.: Lower satellite-gravimetry estimates of Antarctic sea-level contribution, Nature, 491, 586–589, https://doi.org/10.1038/nature11621, 2012.

Lang, C., Fettweis, X., and Erpicum, M.: Stable climate and surface mass balance in Svalbard over 1979–2013 despite the Arctic warming, The Cryosphere, 9, 83-101, https://doi.org/10.5194/tc-9-83-2015, 2015.

https://doi.org/10.5194/egusphere-2026-3461
Preprint. Discussion started: 8 July 2026

Lawrence, D. M., Fisher, R. A., Koven, C. D., Oleson, K. W., Swenson, S. C., Bonan, G., Collier, N., Ghimire, B., van Kampenhout, L., Kennedy, D., Kluzek, E., Lawrence, P. J., Li, F., Li, H., Lombardozzi, D., Riley, W. J., Sacks, W. J., Shi, M., Vertenstein, M., Wieder, W. R., Xu, C., Ali, A. A., Badger, A. M., Bisht, G., van den Broeke, M., Brunke, M. A., Burns, S. P., Buzan, J., Clark, M., Craig, A., Dahlin, K., Drewniak, B., Fisher, J. B., Flanner, M., Fox, A. M., Gentine, P., Hoffman, F., Keppel-Aleks, G., Knox, R., Kumar, S., Lenaerts, J., Leung, L. R., Lipscomb, W. H., Lu, Y., Pandey, A., Pelletier, J. D., Perket, J., Randerson, J. T., Ricciuto, D. M., Sanderson, B. M., Slater, A., Subin, Z. M., Tang, J., Thomas, R. Q., Val Martin, M., and Zeng, X.: The Community Land Model Version 5: Description of New Features, Benchmarking, and Impact of Forcing Uncertainty, Journal of Advances in Modeling Earth Systems, 11, 4245-4287, https://doi.org/10.1029/2018MS001583, 2019.

Li, T., Hofer, S., Moholdt, G., Igneczi, A., Heidler, K., Zhu, X. X., and Bamber, J.: Pervasive glacier retreats across Svalbard from 1985 to 2023, Nature Communications, 16, 705, https://doi.org/10.1038/s41467-025-55948-1, 2025.

Liu, B., King, M., and Dai, W.: Common mode error in Antarctic GPS coordinate time-series on its effect on bedrock-uplift estimates, Geophysical Journal International, 214, 1652-1664, https://doi.org/10.1093/gji/ggy217, 2018.

Loomis, B. D., Luthcke, S. B., and Sabaka, T. J.: Regularization and error characterization of GRACE mascons, Journal of Geodesy, 93, 1381-1398, https://doi.org/10.1007/s00190-019-01252-y, 2019a.

Loomis, B. D., Rachlin, K. E., Wiese, D. N., Landerer, F. W., and Luthcke, S. B.: Replacing GRACE/GRACE-FO C30 With Satellite Laser Ranging: Impacts on Antarctic Ice Sheet Mass Change, Geophysical Research Letters, 47, e2019GL085488, https://doi.org/10.1029/2019GL085488, 2020.

Loomis, B. D., Richey, A. S., Arendt, A. A., Appana, R., Deweese, Y. J. C., Forman, B. A., Kumar, S., Sabaka, T. J., and Shean, D. E.: Water Storage Trends in High Mountain Asia, Frontiers in Earth Science, 7, https://doi.org/10.3389/feart.2019.00235, 2019b.

Lorenzo-Seva, U. and Ten Berge, J. M.: Tucker's congruence coefficient as a meaningful index of factor similarity, Methodology, 2, 57-64, https://doi.org/10.1027/1614-2241.2.2.57, 2006.

Ma, X., Xue, Y., Wang, C., Yi, S., Li, H., TANG, H., Sun, W., and Wang, Q.: Global Evaluation of GRACE Mascon Products in Monitoring Glacier Mass Balance, Authorea Preprints, https://doi.org/10.22541/essoar.173687470.01262738/v1, 2025.

Mantua, N. J., Hare, S. R., Zhang, Y., Wallace, J. M., and Francis, R. C.: A Pacific interdecadal climate oscillation with impacts on salmon production, Bulletin of the American Meteorological Society, 78, 1069-1080, https://doi.org/10.1175/1520-0477(1997)078<1069:APICOW>2.0.CO;2, 1997.

Marzeion, B., Kaser, G., Maussion, F., and Champollion, N.: Limited influence of climate change mitigation on short-term glacier mass loss, Nature Climate Change, 8, 305–308, https://doi.org/10.1038/s41558-018-0093-1, 2018.

Matsuo, K. and Heki, K.: Time-variable ice loss in Asian high mountains from satellite gravimetry, Earth and Planetary Science Letters, 290, 30-36, https://doi.org/10.1016/j.epsl.2009.11.053, 2010.

Maure, D., Kittel, C., Lambin, C., Delhasse, A., and Fettweis, X.: Spatially heterogeneous effect of climate warming on the Arctic land ice, The Cryosphere, 17, 4645-4659, https://doi.org/10.5194/tc-17-4645-2023, 2023.

Maussion, F., Hock, R., Paul, F., Raup, B., Rastner, P., Zemp, M., Andreassen, L., Barr, I., Bolch, T., and Kochtitzky: The Randolph Glacier Inventory Version 7.0 user guide, 8362857, https://doi.org/10.5281/zenodo.8362857, 2023.

Moon, T., Ahlstrøm, A., Goelzer, H., Lipscomb, W., and Nowicki, S.: Rising Oceans Guaranteed: Arctic Land Ice Loss and Sea Level Rise, Current Climate Change Reports, 4, 211-222, https://doi.org/10.1007/s40641-018-0107-0, 2018.

Newman, M., Alexander, M. A., Ault, T. R., Cobb, K. M., Deser, C., Di Lorenzo, E., Mantua, N. J., Miller, A. J., Minobe, S., and Nakamura, H.: The Pacific decadal oscillation, revisited, Journal of Climate, 29, 4399-4427, https://doi.org/10.1175/JCLI-D-15-0508.1, 2016.

Noël, B., van de Berg, W. J., Lhermitte, S., Wouters, B., Schaffer, N., and van den Broeke, M. R.: Six Decades of Glacial Mass Loss in the Canadian Arctic Archipelago, Journal of Geophysical Research-Earth Surface, 123, 1430-1449, https://doi.org/10.1029/2017jf004304, 2018.

Noël, B., Adalgeirsdóttir, G., Pálsson, F., Wouters, B., Lhermitte, S., Haacker, J. M., and van den Broeke, M. R.: North Atlantic Cooling is Slowing Down Mass Loss of Icelandic Glaciers, Geophysical Research Letters, 49, e2021GL095697, https://doi.org/10.1029/2021gl095697, 2022.

Otosaka, I. N., Shepherd, A., Ivins, E. R., Schlegel, N. J., Amory, C., van den Broeke, M. R., Horwath, M., Joughin, I., King, M. D., Krinner, G., Nowicki, S., Payne, A. J., Rignot, E., Scambos, T., Simon, K. M., Smith, B. E., Sorensen, L. S.,

https://doi.org/10.5194/egusphere-2026-3461
Preprint. Discussion started: 8 July 2026

Velicogna, I., Whitehouse, P. L., Geruo, A., Agosta, C., Ahlstrom, A. P., Blazquez, A., Colgan, W., Engdahl, M. E., Fettweis, X., Forsberg, R., Gallée, H., Gardner, A., Gilbert, L., Gourmelen, N., Groh, A., Gunter, B. C., Harig, C., Helm, V., Khan, S. A., Kittel, C., Konrad, H., Langen, P. L., Lecavalier, B. S., Liang, C. C., Loomis, B. D., McMillan, M., Melini, D., Mernild, S. H., Mottram, R., Mouginot, J., Nilsson, J., Noël, B., Pattle, M. E., Peltier, W. R., Pie, N., Roca, M., Sasgen, I., Save, H. V., Seo, K. W., Scheuchl, B., Schrama, E. J. O., Schröder, L., Simonsen, S. B., Slater, T., Spada, G., Sutterley, T. C., Vishwakarma, B. D., van Wessem, J. M., Wiese, D., van der Wal, W., and Wouters, B.: Mass balance of the Greenland and Antarctic ice sheets from 1992 to 2020, Earth System Science Data, 15, 1597-1616, https://doi.org/10.5194/essd-15-1597-2023, 2023.

Papineau, J. M.: Wintertime temperature anomalies in Alaska correlated with ENSO and PDO, International Journal of Climatology, 21, 1577-1592, https://doi.org/10.1002/joc.686, 2001.

Proshutinsky, A., Dukhovskoy, D., Timmermans, M.-L., Krishfield, R., and Bamber, J. L.: Arctic circulation regimes, Philosophical Transactions of the Royal Society A: Mathematical, Physical and Engineering Sciences, 373, https://doi.org/10.1098/rsta.2014.0160, 2015.

Ramos Buarque, S. and Salas y Melia, D.: Link between the North Atlantic Oscillation and the surface mass balance components of the Greenland Ice Sheet under preindustrial and last interglacial climates: a study with a coupled global circulation model, Clim. Past, 14, 1707-1725, https://doi.org/10.5194/cp-14-1707-2018, 2018.

Richard Peltier, W., Argus, D. F., and Drummond, R.: Comment on "An Assessment of the ICE-6G_C (VM5a) Glacial Isostatic Adjustment Model" by Purcell et al, Journal of Geophysical Research: Solid Earth, 123, 2019-2028, https://doi.org/10.1002/2016JB013844, 2018.

Rodell, M., Houser, P. R., Jambor, U., Gottschalck, J., Mitchell, K., Meng, C. J., Arsenault, K., Cosgrove, B., Radakovich, J., Bosilovich, M., Entin, J. K., Walker, J. P., Lohmann, D., and Toll, D.: The global land data assimilation system, Bulletin of the American Meteorological Society, 85, 381–394, https://doi.org/10.1175/bams-85-3-381, 2004.

Rounce, D. R., Hock, R., Maussion, F., Hugonnet, R., Kochtitzky, W., Huss, M., Berthier, E., Brinkerhoff, D., Compagno, L., Copland, L., Farinotti, D., Menounos, B., and McNabb, R. W.: Global glacier change in the 21st century: Every increase in temperature matters, Science, 379, 78-83, https://doi.org/10.1126/science.abo1324, 2023.

Sasgen, I., Salles, A., Wegmann, M., Wouters, B., Fettweis, X., Noël, B. P. Y., and Beck, C.: Arctic glaciers record wavier circumpolar winds, Nature Climate Change, 12, 249-255, https://doi.org/10.1038/s41558-021-01275-4, 2022.

Sasgen, I., Steinhoefel, G., Kasprzyk, C., Matthes, H., Westermann, S., Boike, J., and Grosse, G.: Atmosphere circulation patterns synchronize pan-Arctic glacier melt and permafrost thaw, Communications Earth & Environment, 5, 375, https://doi.org/10.1038/s43247-024-01548-8, 2024.

Save, H., Bettadpur, S., and Tapley, B. D.: High-resolution CSR GRACE RL05 mascons, Journal of Geophysical Research-Solid Earth, 121, 7547-7569, https://doi.org/10.1002/2016jb013007, 2016.

Sun, Y., Riva, R., and Ditmar, P.: Optimizing estimates of annual variations and trends in geocenter motion and J2 from a combination of GRACE data and geophysical models, Journal of Geophysical Research: Solid Earth, 121, 8352-8370, https://doi.org/10.1002/2016JB013073, 2016.

Sutanudjaja, E. H., van Beek, R., Wanders, N., Wada, Y., Bosmans, J. H. C., Drost, N., van der Ent, R. J., de Graaf, I. E. M., Hoch, J. M., de Jong, K., Karssenberg, D., López López, P., Peßenteiner, S., Schmitz, O., Straatsma, M. W., Vannametee, E., Wisser, D., and Bierkens, M. F. P.: PCR-GLOBWB 2: a 5 arcmin global hydrological and water resources model, Geosci. Model Dev., 11, 2429-2453, https://doi.org/10.5194/gmd-11-2429-2018, 2018.

Sutterley, T. C., Velicogna, I., and Hsu, C. W.: Self-Consistent Ice Mass Balance and Regional Sea Level From Time-Variable Gravity, Earth and Space Science, 7, e2019EA000860, https://doi.org/10.1029/2019ea000860, 2020.

Tapley, B. D., Watkins, M. M., Flechtner, F., Reigber, C., Bettadpur, S., Rodell, M., Sasgen, I., Famiglietti, J. S., Landerer, F. W., Chambers, D. P., Reager, J. T., Gardner, A. S., Save, H., Ivins, E. R., Swenson, S. C., Boening, C., Dahle, C., Wiese, D. N., Dobslaw, H., Tamisiea, M. E., and Velicogna, I.: Contributions of GRACE to understanding climate change, Nature Climate Change, 9, 358-369, https://doi.org/10.1038/s41558-019-0456-2, 2019.

Tedesco, M., Fettweis, X., Mote, T., Wahr, J., Alexander, P., Box, J. E., and Wouters, B.: Evidence and analysis of 2012 Greenland records from spaceborne observations, a regional climate model and reanalysis data, Cryosphere, 7, 615-630, https://doi.org/10.5194/tc-7-615-2013, 2013.

https://doi.org/10.5194/egusphere-2026-3461
Preprint. Discussion started: 8 July 2026

Tepes, P., Gourmelen, N., Nienow, P., Tsamados, M., Shepherd, A., and Weissgerber, F.: Changes in elevation and mass of Arctic glaciers and ice caps, 2010-2017, Remote Sensing of Environment, 261, 112481, https://doi.org/10.1016/j.rse.2021.112481, 2021.

Visbeck, M. H., Hurrell, J. W., Polvani, L., and Cullen, H. M.: The North Atlantic Oscillation: past, present, and future, Proceedings of the National Academy of Sciences of the United States of America, 98, 12876-12877, https://doi.org/10.1073/pnas.231391598 2001.

Wang, Q. Y., Yi, S., and Sun, W. K.: Continuous Estimates of Glacier Mass Balance in High Mountain Asia Based on ICESat-1,2 and GRACE/GRACE Follow-On Data, Geophysical Research Letters, 48, e2020GL090954, https://doi.org/10.1029/2020gl090954, 2021.

Wang, Q. Y., Yi, S., Chang, L., and Sun, W. K.: Large-Scale Seasonal Changes in Glacier Thickness Across High Mountain Asia, Geophysical Research Letters, 44, 10427-10435, https://doi.org/10.1002/2017gl075300, 2017.

Watkins, M. M., Wiese, D. N., Yuan, D. N., Boening, C., and Landerer, F. W.: Improved methods for observing Earth's time variable mass distribution with GRACE using spherical cap mascons, Journal of Geophysical Research-Solid Earth, 120, 2648-2671, https://doi.org/10.1002/2014jb011547, 2015.

Wiese, D. N., Landerer, F. W., and Watkins, M. M.: Quantifying and reducing leakage errors in the JPL RL05M GRACE mascon solution, Water Resources Research, 52, 7490-7502, https://doi.org/10.1002/2016wr019344, 2016.

Williams, S. D. P., Moore, P., King, M. A., and Whitehouse, P. L.: Revisiting GRACE Antarctic ice mass trends and accelerations considering autocorrelation, Earth and Planetary Science Letters, 385, 12-21, https://doi.org/10.1016/j.epsl.2013.10.016, 2014.

Wouters, B., Gardner, A. S., and Moholdt, G.: Global Glacier Mass Loss During the GRACE Satellite Mission (2002-2016), Frontiers in Earth Science, 7, 96, https://doi.org/10.3389/feart.2019.00096, 2019.

Wouters, B., Bamber, J. L., van den Broeke, M. R., Lenaerts, J. T. M., and Sasgen, I.: Limits in detecting acceleration of ice sheet mass loss due to climate variability, Nature Geoscience, 6, 613-616, https://doi.org/10.1038/ngeo1874, 2013.

Zemp, M., Huss, M., Thibert, E., Eckert, N., McNabb, R., Huber, J., Barandun, M., Machguth, H., Nussbaumer, S. U., Gartner-Roer, I., Thomson, L., Paul, F., Maussion, F., Kutuzov, S., and Cogley, J. G.: Global glacier mass changes and their contributions to sea-level rise from 1961 to 2016, Nature, 568, 382–386, https://doi.org/10.1038/s41586-019-1071-0, 2019.

Zemp, M., Jakob, L., Dussaillant, I., Nussbaumer, S. U., Gourmelen, N., Dubber, S., A, G., Abdullahi, S., Andreassen, L. M., Berthier, E., Bhattacharya, A., Blazquez, A., Boehm Vock, L. F., Bolch, T., Box, J., Braun, M. H., Brun, F., Cicero, E., Colgan, W., Eckert, N., Farinotti, D., Florentine, C., Floricioiu, D., Gardner, A., Harig, C., Hassan, J., Hugonnet, R., Huss, M., Jóhannesson, T., Liang, C.-C. A., Ke, C.-Q., Khan, S. A., King, O., Kneib, M., Krieger, L., Maussion, F., Mattea, E., McNabb, R., Menounos, B., Miles, E., Moholdt, G., Nilsson, J., Pálsson, F., Pfeffer, J., Piermattei, L., Plummer, S., Richter, A., Sasgen, I., Schuster, L., Seehaus, T., Shen, X., Sommer, C., Sutterley, T., Treichler, D., Velicogna, I., Wouters, B., Zekollari, H., Zheng, W., and The Gla, M. T.: Community estimate of global glacier mass changes from 2000 to 2023, Nature, 639, 382-388, https://doi.org/10.1038/s41586-024-08545-z, 2025.